J. Fluid Mech. (2013), *vol.* 728, *pp.* 120–145. © Cambridge University Press 2013
doi:10.1017/jfm.2013.258

A study of singular modes associated with over-reflection and related phenomena

S. A. Maslowe[1],† **and R. J. Spiteri**[2]

[1]Department of Mathematics, McGill University, Montreal, QC H3A 0B9, Canada
[2]Department of Computer Science, University of Saskatchewan, SK S7N 5C9, Canada

(Received 1 March 2012; revised 25 April 2013; accepted 20 May 2013;
first published online 3 July 2013)

This paper describes an investigation of the linear, diffusive critical layer for shear flows whose inviscid neutral modes have an algebraic branch point. As examples of flows exhibiting such singular behaviour, we treat both stratified shear flows and non-axisymmetric modes on vortices. For the stratified case, the coupled vorticity and energy equations are solved numerically. In this way, the density perturbation, which is unbounded in the absence of diffusion, is determined directly. As an example featuring a vortex, we consider helical modes on a modified Lamb–Oseen vortex whose velocity profile is perturbed in such a way that linear instability is possible. Both the axial and azimuthal velocity perturbations in the critical layer are determined. A characteristic shared by all the above problems is that they involve eigenfunctions that are oscillatory in some region. For forced waves in a stably stratified shear flow, we consider a larger range of parameters than previous investigators. We also examine some experiments and find that the Reynolds stress is sensitive to the actual density profile in the region between a wavy wall providing the forcing and the critical layer. For the stratified shear flows without forcing, much smaller Richardson numbers are involved and the modes considered are over-reflecting. For an unbounded $\tanh y$ mixing layer, we show that the Reynolds stress for a neutral mode must jump across the critical layer. With the presence of a horizontal boundary beneath the shear layer, on the other hand, over-reflection can occur, with the Reynolds stress vanishing on either side of the critical layer. In all cases, the variation of the Reynolds stress across the critical layer is determined.

Key words: critical layers, stratified flows, vortex instability

1. Introduction

The important role of the Reynolds stress variation in shear flows, particularly within thin ‘critical layers’, has been appreciated for many years in the context of hydrodynamic stability. Viscosity is significant within such layers even when the Reynolds number is so large that its effect is negligible elsewhere. An impressive illustration can be seen in figure 8 of the survey article by Stuart (1963) showing the Reynolds stress variation across a channel for a slightly amplified mode in plane

† Email address for correspondence: maslowes83@gmail.com

https://doi.org/10.1017/jfm.2013.258 Published online by Cambridge University Press

Poiseuille flow. The figure shows clearly that the Reynolds stress has a sharp peak near the critical point, located at that value of y where the phase speed $c = \bar{u}(y)$, the mean flow velocity.

This paper addresses a number of essentially inviscid shear flow problems, having in common that the role of the critical layer is significant in each case. Both stratified shear flows and vortices are investigated. For a stratified laminar shear flow, a sufficient condition for stability is that the local Richardson number (defined in § 2) be everywhere greater than 1/4. (Galperin, Sukoriansky & Anderson 2007 point out that turbulence is still possible if conditions assumed in the derivation of the Richardson number 1/4 theorem, such as a steady flow, are not satisfied.) We first consider shear flows that are stable according to this criterion with the wave motion a consequence of spatially periodic forcing at one of the boundaries. Considerable interest in such problems followed the results published by Booker & Bretherton (1967) who considered the linear initial-value problem for a flow with constant shear and buoyancy frequency in the region containing the critical layer. The forcing was switched on at the lower boundary at time $t = 0$, thereby inducing a vertical wave propagation towards the critical layer. A Laplace transform was employed to deal with the time dependence and an asymptotic analysis, valid as $t \to \infty$, suggested that most of the wave energy would be absorbed in the critical layer. Specifically, if J_c is the local Richardson number at the critical point, then the Reynolds stress and associated momentum flux were shown to be attenuated by a factor $\exp\{-2\pi(J_c - 1/4)^{1/2}\}$ as the critical layer is crossed. This suggests that most of the wave energy is absorbed in the critical layer and transferred there to the mean flow, which will then be modified.

The critical layer absorption described above begins once the time is sufficiently large that the flow in the critical layer has become quasi-steady and the notion of a phase change across the critical point y_c is then applicable. The latter term is associated with singular neutral modes in the classical theory, but it is equally pertinent to modes whose amplitude is evolving slowly. For shear flows having a branch point y_c in their power series representations, the branch point terms are written $(y - y_c)$ for $y > y_c$ and $|y - y_c|e^{i\phi}$ below the critical point. Within the framework of linear theory, the phase change ϕ can be determined either by introducing a diffusive critical layer centred on the point y_c or by employing a Laplace transform in the inviscid initial-value problem. In either approach, the result obtained is that $\phi = -\mathrm{sign}(\bar{u}_c')\pi$, where $\bar{u}_c' = \bar{u}'(y_c)$.

As t becomes large, the linear initial-value analysis for forced waves breaks down near the critical layer and, in the case of a stratified shear flow, both the horizontal perturbation velocity and the density perturbation tend towards infinity at the critical point. Either nonlinearity or diffusive effects (viscosity and heat conduction) must be included in the critical layer once the aforementioned perturbations become large. The appropriate choice depends on which is the larger of the two critical layer thicknesses: $\varepsilon^{2/3}$, the nonlinear critical thickness or $(\alpha Re)^{-1/3}$, the thickness of the diffusive critical layer (Maslowe 1986); ε here is a dimensionless perturbation amplitude parameter, α the wavenumber and Re is the Reynolds number. A number of studies, both analytical and computational, have been carried out to investigate the nonlinear regime following work on the corresponding forced Rossby wave problem. In atmospheric applications, Re is typically very large so nonlinearity is the relevant choice rather than molecular diffusion. Brown & Stewartson, in a series of articles, improved the analysis of Booker & Bretherton and investigated the initial effects of nonlinearity by expanding in powers of a slow time scale $\tau = \varepsilon^{2/3}t$. In so doing, they found evidence

https://doi.org/10.1017/jfm.2013.258 Published online by Cambridge University Press

of a weak transmitted wave and a considerably stronger reflected wave. This work is summarized in the review article by Stewartson (1981).

The present article is focused on the linear, diffusive critical layer. This limit has received less attention, which is surprising, because it is likely to be the appropriate limit in many experiments. In the atmosphere, Re is often very large because length scales based on the width of the shear layers responsible for Kelvin–Helmholtz billows can be of the order of several hundred metres. Clearly, this is not possible in the laboratory, where Re must be much smaller not only because of the length scale but also because the kinematic viscosity of fluids employed in experiments is greater than that of air.

If diffusive effects are used to resolve the singularities arising in the linear inviscid theory, then a single sixth-order differential equation can be derived for the y component of the vertical velocity perturbation. This equation was solved numerically by Hazel (1967), who confirmed that the phase change obtained from the steady, diffusive critical layer analysis was the same as that resulting from the $t \to \infty$ limit of the inviscid initial-value problem. This supports the conclusion of Booker & Bretherton (1967) that little of the incoming wave energy is transmitted or reflected. Of particular interest in Hazel's paper is a figure illustrating the computed Reynolds stress variation in the critical layer for what was identified only as a 'typical solution'. Tabulated results were also presented for a few cases, apparently to make qualitative comparisons with an experiment described in the appendix. The tabulated cases were for values of Richardson number $3.0 \leqslant J_c \leqslant 4.0$ and Prandtl number $1.1 \leqslant Pr \leqslant 7.0$. Computational difficulties limited J_c at the upper end and we have repeated some of Hazel's computations employing more robust numerical methods. A larger range of Richardson numbers is considered and we also include results for $Pr = 0.72$, the value for air.

The second class of problems that we consider, in contrast with the first, is composed of shear flows for which the minimum value of the local Richardson number is less than $1/4$. Linear instability is therefore possible according to the Miles–Howard theorem. We are interested specifically in modes associated with instabilities whose existence is related to their eigenfunctions being somewhere oscillatory. These include modes whose instability can be attributed to the over-reflection mechanism. Chapter 2 of the monograph by Craik (1985) contains an excellent review of this novel topic and the principal references are cited therein. What attracted so much interest to this phenomenon is that a mode propagating vertically towards a critical layer is apparently reflected with more energy than it had initially. Eltayeb & McKenzie (1975) investigated the specific case of the broken-line approximation to a hyperbolic tangent mixing layer and showed that over-reflection can occur only for $J_c < 0.1129$. Lindzen & Barker (1985) discuss thoroughly the conditions most favourable for over-reflection to occur in stratified shear flows.

Despite the extensive literature treating over-reflection and the agreement about the essential role of a critical layer, none of these papers investigates the critical layer structure or the Reynolds stress variation, as was done by Hazel in the forced wave case. We have therefore re-examined several of the papers cited by Craik and, in addition to solving the critical layer equations, we have obtained more accurate solutions of the outer eigenvalue problem. The computational issue is the presence of the singularity y_c in the governing Taylor–Goldstein equation. Other researchers, such as Lalas & Einaudi (1976), have either used Frobenius solutions to cross y_c or else computed only amplified modes, as was done by Drazin, Zaturska & Banks (1979). Both papers considered the stratified shear flow with velocity profile $\bar{u} = \tanh y$

https://doi.org/10.1017/jfm.2013.258 Published online by Cambridge University Press

and constant buoyancy frequency. The paper of Lalas & Einaudi (1976) explored the interesting effect of a lower boundary. The growth rates are small for over-reflected modes so the singularity is near the real axis. We employed an indented contour to carry out the integrations, thereby avoiding difficulties related to the critical point.

As a final example, we investigate the viscous critical layer for singular modes propagating on a vortex. Despite the geometrical differences, Le Dizès (2004) showed recently that the critical layer equation for the pressure perturbation in a vortex is the same as that governing the vertical velocity in a stratified shear flow. Although the two equations are the same when $Pr = 1$, differences in the outer problem mean that the boundary conditions can be quite different in the two cases. In § 5, we solve this sixth-order equation for a neutral mode propagating on a modified Lamb–Oseen vortex and we compute the Reynolds stress in the critical layer.

2. The governing equations

We consider the linear theory for small two-dimensional perturbations to a stratified shear flow with velocity and density profiles $\bar{u}(y)$ and $\bar{\rho}(y)$, respectively. The governing equations incorporate the Boussinesq approximation and within this framework it is convenient to employ as a starting point the non-dimensional continuity, vorticity and energy equations. After linearizing, the equations governing the perturbation quantities $\hat{u}$, $\hat{v}$ and $\hat{\rho}$ can be written

$$\alpha\,\hat{u}_\xi + \hat{v}_y = 0, \tag{2.1}$$

$$(\bar{u} - c)\,\hat{\omega}_\xi - \frac{\bar{u}''}{\alpha}\,\hat{v} + \frac{g}{\bar{\rho}}\,\hat{\rho}_\xi = \frac{1}{\alpha Re}\,\nabla^2\hat{\omega}, \tag{2.2}$$

$$(\bar{u} - c)\,\hat{\rho}_\xi + \frac{\bar{\rho}'}{\alpha}\,\hat{v} = \frac{1}{\alpha RePr}\,\nabla^2\hat{\rho}, \tag{2.3}$$

where $\xi = \alpha(x - ct)$ and $g = g_0 L/V^2$. The wavenumber α is real, whereas c is generally complex, its real part being the perturbation phase speed, g_0 is the gravitational constant, L is a length scale for the velocity profile (usually the half-width of the shear layer) and V is a characteristic velocity. Finally, $\hat{\omega} = \alpha\,\hat{v}_\xi - \hat{u}_y$ denotes the perturbation vorticity.

A few words about (2.1)–(2.3) are appropriate because the Boussinesq approximation entails slightly more in the diffusive equations than it does in the inviscid version and we will deal with both. The neglect of inertial terms in (2.2) while retaining buoyancy is, of course, the primary assumption in both cases. Where slight differences arise is that the energy equation is part of the diffusive system so the temperature T appears initially as a dependent variable rather than the density, the natural choice in inviscid problems. Fortunately, the equation of state normally employed in the diffusive theory is of the form $\rho(T) = \rho_0[1 - \gamma(T - T_0)]$, where the constants ρ_0 and T_0 are reference states and γ is the coefficient of thermal expansion. Because the density is independent of pressure, we can replace T with ρ in (2.3); Chapter 1 of the monograph by Baines (1995) is a useful reference for details of the derivation.

A separation of variables is achieved by writing all perturbation quantities in the form $f(y)\exp\{\mathrm{i}\xi\}$. The dependent variables $u(y)$, $v(y)$, and $\rho(y)$ will denote, respectively, the y-dependent component of the horizontal and vertical velocities, and the density. After substituting into (2.1)–(2.3), a single equation can be obtained for $v(y)$. If we assume that the mean density is of the form $\bar{\rho} = \exp\{-\beta\bar{r}(y)\}$, the resulting

https://doi.org/10.1017/jfm.2013.258 Published online by Cambridge University Press

equation, often termed the Taylor–Goldstein equation, can be written

$$\frac{\mathrm{d}^2 v}{\mathrm{d}\, y^2} - \left[\alpha^2 + \frac{\bar{u}''}{(\bar{u}-c)} - \frac{\bar{r}' J_0}{(\bar{u}-c)^2}\right] v = 0, \tag{2.4}$$

where $J_0 = g\beta$ is the overall Richardson number. From the standpoint of stability theory, the principal result that follows from (2.4) is the necessary condition for instability derived by Miles (1961) and generalized by Howard (1961), namely, that the local Richardson number $J(y) = J_0\, \bar{r}'/\bar{u}'^2$ be somewhere less than $1/4$. It was shown, in addition, that $(\bar{u} - c) \to 0$ for neutral modes that are the limit of unstable solutions as $c_i \to 0$.

The last remark is especially pertinent to our study, because c_i will be either small or zero in both classes of problems that we consider, albeit for different reasons. Given that the critical point singularity will be either on or near to the real y-axis, the approach of Miles (1961) based on Frobenius expansions centred on y_c is essential to our analysis. Following his approach, all variable coefficients in (2.4) are expanded around the critical point y_c to obtain a solution valid locally having the form

$$v(y) = A\, v_+(y) + B\, v_-(y), \tag{2.5}$$

where

$$v_\pm(y) = (y - y_c)^{(1\pm\nu)/2}\, w_\pm(y) \tag{2.6}$$

and the functions $w_\pm(y)$ are regular in the neighbourhood of y_c; the parameter ν in (2.6) is related to J_c by $\nu = (1 - 4J_c)^{1/2}$ for $J_c < 1/4$. Although $v(y) \to 0$ as $y \to y_c$, it will be seen below that the density perturbation becomes infinite. When the flow is stable with $J_c > 1/4$, as in the forced wave problem of Booker & Bretherton, it is more convenient to employ the real constant μ in the Frobenius exponent, where $\nu = 2\mathrm{i}\mu$. (Because we will compare our results with those of Hazel, we use his definition of μ rather than that of Miles, which is smaller by a factor of 2.)

With the exception of the special value $J_c = 1/4$, the scaling of the critical layer equations and matching with the outer region is somewhat different in the two situations studied in the following sections. We will, therefore, provide the details separately for each case. It is worth noting, however, that as $y \to y_c$, the density perturbation $\rho \to \infty$. This follows from the inviscid limit of (2.3) which, after separating variables, yields

$$\rho(y) = \frac{\mathrm{i}\,\bar{\rho}'}{\alpha\,(\bar{u} - c)}\, v(y). \tag{2.7}$$

Moreover, from the continuity equation (2.1), it is clear that the behaviour of u, the horizontal perturbation, is the same near y_c as that of ρ. This is significant because of the importance of the Reynolds stress, which involves the product uv. For neutral modes, the Reynolds stress is a constant, independent of y, but this constant can jump across critical points. We will say more about this below, when we deal with specific cases. That said, let us proceed now to the stable, forced wave problem.

Using arguments based on the variation of the Reynolds stress, Miles (1961) proved a number of useful results that apply to singular neutral modes. For example, within the framework of linear theory, a neutral mode comprising part of a stability boundary must be proportional to one or the other of the Frobenius solutions. With the exception of profiles that are specially constructed to avoid dealing with critical points, there is a $-\pi$ phase change as y_c is crossed and this is true whether the initial-value approach is used or diffusive effects are restored within a critical layer.

https://doi.org/10.1017/jfm.2013.258 Published online by Cambridge University Press

For the two classes of problems considered in this paper, the properties of neutral or slightly amplified modal solutions of (2.4) are the main focus.

3. The diffusive critical layer for stratified flows with $J_c > 1/4$

In this section, we investigate the structure of a linear critical layer of thickness $O(\alpha Re)^{-1/3}$ within which the leading-order diffusive terms in (2.2) and (2.3) are retained. It will be seen that there are computational advantages to solving the coupled fourth-order vorticity equation and second-order energy equation rather than the sixth-order equation derived by Koppel (1964). Asymptotic conditions are employed to match to the inviscid outer problem which, in the time-dependent problem, is composed of both upward and downward propagating waves. Booker & Bretherton used group velocity arguments to show that the first Frobenius solution in (2.5), which is now written $(y - y_c)^{1/2+i\mu}$, represents an upward propagating wave, whereas the second solution should be interpreted as a downward propagating wave. (As noted below (2.6), $\mu = (J_c - 1/4)^{1/2}$.)

Because none of the dependent variables is $O(1)$ as $y \to y_c$, we must rescale the dependent variables in the critical layer, making use of the Frobenius expansions. We will retain the normalization employed in Hazel (1967) and provide details missing from his paper; one reason is that we solve three critical layer equations rather than a single equation for the vertical velocity. Recalling that the forced initial value problem involves the introduction of a wavy boundary below the critical layer at time $t = 0$, the upward propagating wave is the primary focus. It is convenient to normalize this wave above the critical layer even though little of it passes through. Suppose then that for $y > y_c$, the outer solution is written $v_0 (y - y_c)^{1/2+i\mu}$. It can be verified that for the inner variables defined below, the appropriate choice for the arbitrary constant is $v_0 = (\alpha \bar{u}_c' Re)^{i\mu/6}$. Consistent with the foregoing choice of v_0, we define the dependent variables in the critical layer as follows:

$$u(y) = \frac{\Gamma^{1/6}}{i\alpha} U(Y), \quad v(y) = \frac{1}{\Gamma^{1/6}} V(Y) \quad \text{and} \quad \rho(y) = \frac{i\bar{\rho}_c'}{\Gamma^{1/6}} R(Y), \tag{3.1}$$

where

$$\Gamma \equiv \alpha \bar{u}_c' Re \quad \text{and} \quad Y = \Gamma^{1/3} (y - y_c). \tag{3.2}$$

With the scaling in (3.1)–(3.2), substituting into the separated versions of (2.1)–(2.3) leads to the critical layer equations which, to leading order, are given by

$$\frac{dV}{dY} + U = 0, \tag{3.3}$$

$$\frac{d^4V}{dY^4} - iY\frac{d^2V}{dY^2} = iJ_c R \tag{3.4}$$

and

$$\frac{d^2R}{dY^2} - iPr\, YR = -iPr\, V. \tag{3.5}$$

We must solve the boundary-value problem associated with the coupled ordinary differential equations (ODEs) (3.4) and (3.5); U is given simply by (3.3) once the solution has been obtained for $V(Y)$. The boundary conditions are provided by matching to the outer inviscid problem. The solution below the critical layer, in general, is composed of a forced upward propagating wave and a reflected wave,

https://doi.org/10.1017/jfm.2013.258 Published online by Cambridge University Press

whose amplitude is unknown. The matching condition to be satisfied by V can therefore be written

$$V \sim -\mathrm{i}|Y|^{1/2}\mathrm{e}^{\mu\pi}\mathrm{e}^{\mathrm{i}\mu\log|Y|} + A\mathrm{e}^{-\mu\pi}|Y|^{1/2}\mathrm{e}^{-\mathrm{i}\mu\log|Y|} \quad \text{as } Y \to -\infty. \tag{3.6}$$

Implicit in (3.6) is both the normalization utilized by Hazel, which follows from (2.8) in Booker & Bretherton (1967), and the $-\pi$ phase change of linear critical layer theory, as presented in (3.18b) of Miles (1961). A word about the phase change is appropriate here. Baldwin & Roberts (1970) extended the earlier work of Koppel and showed that the $Re \to \infty$ limit of the diffusive problem yields the same phase change as that obtained by Booker & Bretherton. It is not necessary to assume this *a priori*; we could have determined the transmission coefficient of the upward wave during the computation in the same way that we will find the reflection coefficient, A in (3.6). This is essentially what was done by Hazel and we have done so in a few cases to verify our solution procedure. In any case, we take as the solution for V above the critical layer

$$V \sim Y^{1/2}\mathrm{e}^{\mathrm{i}\mu\log Y} \quad \text{as } Y \to \infty. \tag{3.7}$$

Finally, we must state the asymptotic matching conditions for the density R. From (3.5), it is readily deduced that

$$R \sim \frac{V}{Y} \quad \text{as } Y \to \pm\infty. \tag{3.8}$$

By substituting the large-$|Y|$ behaviour of V into (3.8), it is easy to see that R'' can be neglected in (3.5) for $|Y| \gg 1$. This is one reason why it is easier to solve the pair of differential equations (3.4) and (3.5) rather than the single sixth-order equation that would result from combining them.

3.1. *Numerical solution procedure and some results*

The procedure employed in Hazel (1967) was to use a Runge–Kutta method to integrate the governing equation inward from above and below the critical layer and to then match the two solutions at $Y = 0$. The WKBJ method was used to obtain linearly independent solutions, valid for large $|Y|$, that provide starting conditions for the integration (see, also, Baldwin & Roberts 1970). After rejecting exponentially growing solutions, there remained four solutions below the critical layer and three above that were superimposed to obtain the complete solution. Among the numerical difficulties encountered was that the starting distance could not be too large or too small owing to the exponential behaviour of the viscous solutions. From (3.18b) of Miles (1961), we know that the reflection coefficient $A = 0$ because in the steady case a wave propagating downward below the critical layer would imply an incoming wave from infinity. Hazel (1967) included the reflected wave as a measure of computational error and we have done the same. More will be said about this in § 3.2.

The procedure we employ is based on a formulation of (3.4)–(3.8) as a boundary-value problem followed by the use of MATLAB's boundary-value problem solver `bvp5c` (Kierzenka & Shampine 2008). The numerical method underpinning `bvp5c` is collocation using the four-point Lobatto IIIA formula. Error control and mesh selection are based on a scaled residual, i.e. a measure of the amount by which the continuous extension of the numerical solution fails to satisfy the differential equations. However, a nice feature of `bvp5c` is that the scaled residual is an asymptotically correct approximation to the size of the true error; hence `bvp5c` can be considered

https://doi.org/10.1017/jfm.2013.258 Published online by Cambridge University Press

in effect to control the true error. Because `bvp5c` is designed to handle first-order systems, we convert (3.4)–(3.5) to a system of six first-order ODEs in the dependent variables V, V', V'', V''', R, and R'.

To obtain an initial guess for the solution, we solve the closely related problem applying when $Pr = 1$. In particular, Gage & Reid (1968) showed that the governing sixth-order equation for $V(Y)$ can be factorized into a product of two third-order equations, either of which can be written

$$\frac{\mathrm{d}^3 V}{\mathrm{d}Y^3} - \mathrm{i}Y\frac{\mathrm{d}V}{\mathrm{d}Y} + \mathrm{i}pV = 0, \tag{3.9}$$

where p is one of the Frobenius exponents. Knowing that the reflected wave is weak and only numerical, we neglect it below the critical layer in the approximate solution by setting $A = 0$ in (3.6) and making the choice $p = 1/2 + \mathrm{i}\mu$. A second boundary condition below the critical layer can be obtained by differentiating (3.6) once. Finally, the third boundary condition is provided by imposing the condition that there is only an outgoing wave above the critical layer. Although the amplitude of this outgoing wave is not known, (3.7) can be differentiated once to find the radiation condition

$$\frac{\mathrm{d}V}{\mathrm{d}Y} - \left(\frac{\mathrm{i}\mu + 1/2}{Y}\right) V = 0 \quad \text{as } Y \to \infty. \tag{3.10}$$

We have solved the boundary-value problem outlined above for a variety of values of the Richardson and Prandtl numbers. Given that the qualitative behaviour of the solutions was similar in all cases, we present results for only one case in order to complement those given in Hazel (1967). The Reynolds stress variation and behaviour of $V(Y)$ in figure 1 are similar to those in figure 2 of Hazel which were, presumably, for $J_c = 3$ and $Pr = 7$. One minor difference that we should point out is that the entire curves shown, including those for large negative Y, were obtained from solving the critical layer equations. In figure 2 of Hazel, on the other hand, for $-Y > 6$ the asymptotic inviscid solution was apparently patched to his numerical critical layer solution computed for $-6 < Y < 6$. It should also be noted that our Reynolds stress has the opposite sign compared with Hazel (1967). We have used the same definition as Miles (1961), namely, $\tau = -\overline{\hat{u}\hat{v}}$ which in terms of the critical layer variables (3.1) and (3.2) is given by

$$\tau = \frac{1}{2\alpha}(U_r V_i - U_i V_r). \tag{3.11}$$

The subscripts r and i denote, of course, the real and imaginary parts.

It is more interesting to look at $R(Y)$, the density perturbation, than $V(Y)$ because it can be seen from (2.7) that without diffusion the density would become unbounded at the critical point, whereas $v \to 0$. Figure 2 illustrates the behaviour of $|R|(Y)$ in the critical layer and this quantity does become very large near $Y = 0$ on the side of the incoming wave. Although we do not show the solutions for other values of J_c, the maximum value of $|R|$ was observed to scale approximately with $\mathrm{e}^{\mu\pi}$; this would be the expectation based on the behaviour of the inviscid solution. The increase in $|R|_{max}$ with increasing J_c is, however, slightly less than this expectation. For example, when $J_c = 3$, $|R|_{max} = 92$. Multiplying this value by $\mathrm{e}^{\mu\pi}$, would give a value of approximately 3158. However, it can be seen in figure 2 that the actual value of $|R|_{max}$ is about 18 % smaller. A likely explanation is that the steeper gradients of the velocity as J_c increases makes viscosity more effective in damping large quantities such as U and R in the critical layer.

https://doi.org/10.1017/jfm.2013.258 Published online by Cambridge University Press

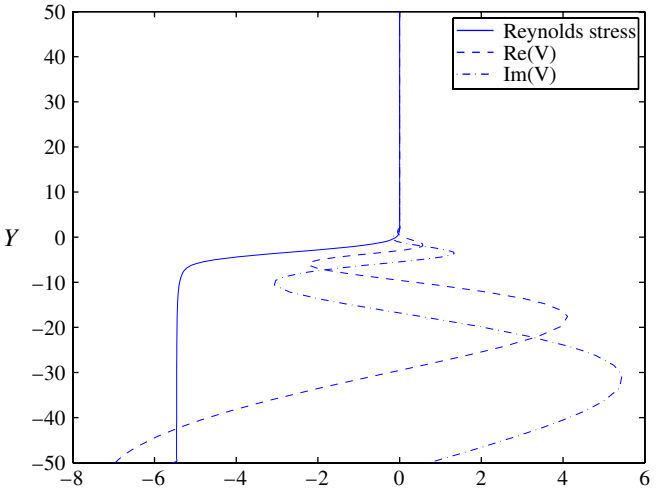


FIGURE 1. (Colour online) Variation of the Reynolds stress and the vertical velocity perturbation in the case of Richardson number $J_c = 8$ and Prandtl number $Pr = 0.72$.

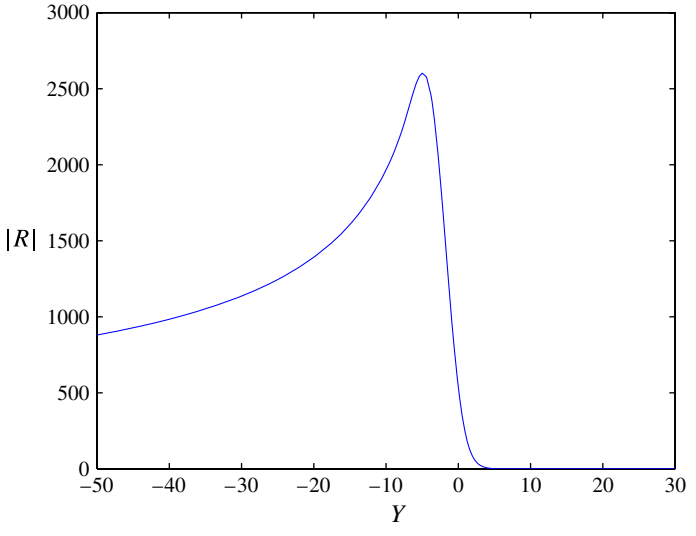


FIGURE 2. (Colour online) Variation of the modulus of the density perturbation in the case of Richardson number $J_c = 8$ and Prandtl number $Pr = 0.72$.

3.2. *Some comparisons with an experiment*

The formulation above is appropriate for situations in which there is only weak coupling between the critical layer dynamics and the source of the upward propagating forced wave. In simulating experiments, however, because of the length and time scales involved, more of the flow domain must be considered. Because our analysis is steady, there are boundary conditions to be satisfied both at the edge of the critical layer and at the lower boundary, where there is a monochromatic forcing. The experiments that we chose to model were those reported by Delisi & Dunkerton

https://doi.org/10.1017/jfm.2013.258 Published online by Cambridge University Press

(1989). The reason for choosing these experiments, in particular, is that the authors provide detailed velocity and density profiles and the observations were made over times much longer than in earlier experiments. In addition, the distorted velocity profile was illustrated at various times.

The forcing, as envisaged by Booker & Bretherton (1967), was due to a stationary sinusoidal boundary located at $y = 0$. In the experiments of Delisi & Dunkerton (1989), however, the boundary was moving so as to produce a wave disturbance with a velocity of 4.5 cm s^{-1} and the critical point was 26.7 cm above the forcing. The Brunt–Väisälä frequency, $N = (-g_0\,\bar{\rho}'/\bar{\rho})^{1/2}$ was not constant, as assumed in many numerical simulations, but it was nearly constant in the lower half of the apparatus. Given that we are interested primarily in the region near the critical layer, we non-dimensionalized the velocity and density profiles using the phase speed of the disturbance to scale velocity, along with a length scale $L = 4.76$ cm characteristic of the shear at the critical point. Corresponding to that choice, $\bar{u}_c' = 1$ and the Richardson number at the critical point $J_c = 2.52$. With these considerations, the dimensionless velocity and Brunt–Väisälä frequency profiles we used are the following:

$$\bar{u}(y) = \mathrm{e}^{y-5.606} \quad \text{and} \quad N^2(y) = \begin{cases} 0.7716, & 0 \leqslant y \leqslant 3.0 \\ 0.6709(y - 1.85), & 3.0 < y < 5.606. \end{cases} \tag{3.12}$$

Our procedure was to begin by solving the Taylor–Goldstein equation (2.4) in the domain $0 \leqslant y \leqslant 5.0$ using the above profiles. The lower boundary condition, as in Booker & Bretherton (1967), was $\hat{v}(x, 0) = v_0 \cos \alpha x$ (i.e. $v(0) = v_0$) corresponding to the prescribed forcing, and at $y = 5.0$ we matched to the critical layer solution. As before, for generality, we included a reflected wave in addition to the upward propagating wave generated by the forcing. Matching the inner and outer solutions at a particular value of Y essentially prescribes the Reynolds number for a given wavenumber α, i.e. $Y = (\alpha \bar{u}_c' Re)^{1/3}(y - y_c)$, where $y_c = 5.606$. We chose a relatively large value of $|Y|$ to do the matching in order to reduce the magnitude of the reflected wave. As discussed below figure 3 of Hazel (1967), the numerical error is largely associated with neglecting the Y^{-3} term in the expansion of the critical layer equations for $|Y| \gg 1$. We found that the magnitude of the reflected wave, which was approximately 3 % of the input wave when matching at $Y = -12$, was reduced to less than 1 % if we matched at $Y = -18$.

As for the boundary conditions used to solve (3.3)–(3.5), below the critical layer it should be noted that the magnitude of the incoming wave is now proportional to v_0, the forcing amplitude. Writing the lower matching condition as

$$V = B_1 |Y|^{1/2} \mathrm{e}^{\mathrm{i}\mu \log |Y|} + A_1 \mathrm{e}^{-\mu\pi} |Y|^{1/2} \mathrm{e}^{-\mathrm{i}\mu \log |Y|}, \tag{3.13}$$

the amplitude B_1 of the input wave is obtained from the solution of the Taylor–Goldstein equation. The coefficient of the reflected wave is unknown, but it can be eliminated from the matching condition by differentiating (3.13) to obtain

$$|Y| \frac{\mathrm{d}V}{\mathrm{d}|Y|} - \left(\frac{1}{2} - \mathrm{i}\mu\right) V = 2\mathrm{i}\mu\, B_1 |Y|^{1/2} \mathrm{e}^{\mathrm{i}\mu \log |Y|}. \tag{3.14}$$

We require U to compute the Reynolds stress, and from (3.3) $U = -\mathrm{d}V/\mathrm{d}Y = \mathrm{d}V/\mathrm{d}|Y|$. The asymptotic condition above the critical layer is (3.10), as before, allowing only a transmitted wave. If the matching condition (3.13) is compared with (3.6), used by Hazel and earlier by ourselves, it can be seen that the normalization has been changed slightly and that is because we observed that the spurious reflected wave is now larger.

https://doi.org/10.1017/jfm.2013.258 Published online by Cambridge University Press

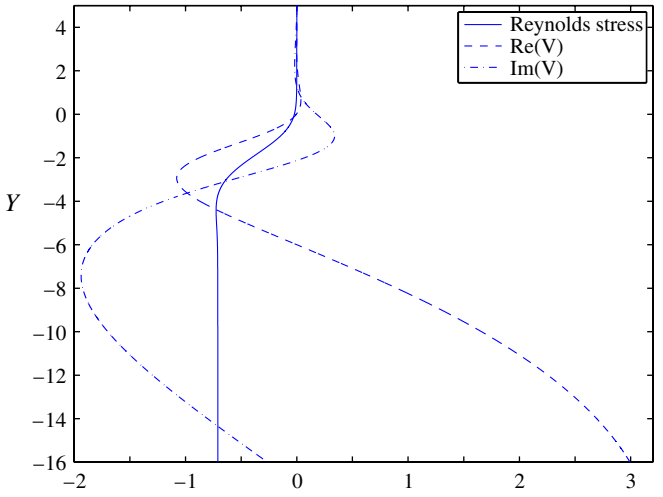


FIGURE 3. (Colour online) Variation of the Reynolds stress and the vertical velocity perturbation in experiments with Richardson number $J_c = 2.52$. The wavenumber $\alpha = 0.60$ for this case.

Whereas the difference in magnitude between the incoming and the reflected wave was assumed to be $e^{-2\mu\pi}$ in (3.6), it has now been reduced to $e^{-\mu\pi}$. This appears to be a consequence of the parameters and finite dimensions of the experiment that we are modelling.

In figure 3, we show the solution for $V(Y)$ and the Reynolds stress $\tau(Y)$ for a case typical of those we ran. The forcing amplitude was chosen to be $v_0 = 1.0$. The Reynolds number and Prandtl number for the experiments were not given in Delisi & Dunkerton (1989), but the results were qualitatively similar for all values that we tried. (As pointed out by a referee, the Schmidt number rather than the Prandtl number would be used if we were actually doing a quantitative comparison with the experiment, where a stratified salt solution was employed.) What was most interesting, however, was the sensitivity that we noticed to the density profile. Just for comparison we wondered what would happen had we employed a constant Brunt–Väisälä frequency, namely, the value at the critical point y_c. In that case, the Reynolds stress below the critical layer was $\tau = -1.19$, compared with $\tau = -0.706$ for the case illustrated in figure 3 using the experimental density profile.

We conclude this section with an approximate analysis of the distortion of the mean velocity profile. Figure 10 of Delisi & Dunkerton (1989) shows that in the experiments, the velocity was significantly accelerated not only below the critical layer, but all the way to the moving boundary at $y = 0$. Clearly, direct quantitative comparisons between our steady, linear solution and the experiments cannot be made for a number of reasons. First, the amplitude of the forcing was substantial. But, more importantly, even after 75 min, the mean flow was oscillating rapidly in the experiments. It is nonetheless of interest to examine the equation governing the evolution of the mean flow.

Including time dependence and viscosity, we follow §2.2 of Campbell (2004) and write the total horizontal velocity as $\bar{u}(y) + u_0(y, t)$, where $\bar{u}(y)$ is the undisturbed velocity profile. After averaging over one wavelength, the momentum equation for the

https://doi.org/10.1017/jfm.2013.258 Published online by Cambridge University Press

wave-induced velocity distortion can be written

$$\frac{\partial u_0}{\partial t} - \frac{\partial \tau}{\partial y} = -\frac{\partial \bar{p}}{\partial x} + \frac{1}{Re}\frac{\partial^2 u_0}{\partial y^2}. \tag{3.15}$$

In weakly nonlinear analyses, τ is $O(\varepsilon^2)$ and it can be estimated from the linear solution. Neglecting the higher harmonics while retaining the interaction between the mean flow and basic disturbance is sometimes called the quasi-linear approximation. Stuart (1963, p. 566) discusses this approximation, as well as the derivation of the mean motion equation. Both the mean flow and the pressure are, as a consequence of the non-zero Reynolds stress, modified by terms of $O(\varepsilon^2)$. However, even without doing a weakly nonlinear analysis, we can make some qualitative observations about the mean flow distortion by using the linear results to approximate the Reynolds stress. For example, according to our solution (see figure 3), $\partial\tau/\partial y$ is positive in the critical layer and for early times this would produce an acceleration of the mean flow, as observed in the experiments.

Even though a steady state was not reached in the experiments of Delisi & Dunkerton (1989), it is of interest to see what can be learned from (3.15). The derivative of the averaged pressure is zero and recalling that $\tau \sim O(\varepsilon^2)$, we can write the governing equation for the wave-induced contribution to the mean horizontal velocity as

$$-\varepsilon^2 \frac{\mathrm{d}\hat{\tau}}{\mathrm{d}y} = \frac{1}{Re}\frac{\mathrm{d}^2 u_0}{\mathrm{d}y^2}, \tag{3.16}$$

where $\tau = \varepsilon^2\hat{\tau}$. Given that (3.16) is a second-order differential equation, there are only two boundary conditions that can be imposed. The first, and more obvious of the two, is that above the critical layer $u_0 = 0$. Figure 3 shows $\tau(Y)$ in the critical layer, where we recall from (3.2) that $Y = \Gamma^{1/3}(y - y_c)$, where $\Gamma = \alpha\bar{u}_c' Re$. Our procedure is to choose an initial value $Y = Y_0$, say, where the condition of zero distortion is imposed and (3.16) is then integrated downwards to some large negative value of Y, where τ has become constant. The solution of (3.16) can then be written

$$\Gamma^{1/3} u_0(\bar{Y}) = -\varepsilon^2 Re \int_0^{\bar{Y}} \hat{\tau}\,(Y^*)\,\mathrm{d}Y^* + C_1\bar{Y}, \tag{3.17}$$

where $\bar{Y} = Y_0 - Y$.

Below the critical layer, the flow is presumed inviscid and τ must then be constant for a neutral mode. From the critical layer solution depicted in figure 3, we see that this is the case and we denote this negative constant $\hat{\tau}_1$. It is now clear that we must choose $C_1 = \varepsilon^2\hat{\tau}_1 Re$; otherwise, u_0 would become unbounded as $\bar{Y} \to \infty$. Below the value of $\bar{Y}$ where the critical layer solution is matched to the inviscid outer region, we set u_0 to be a constant; this is a solution of (3.16) consistent with a constant Reynolds stress.

Figure 4 shows a typical result that was obtained using $Re = 3834$, $\alpha = 0.6$ and $\varepsilon = 0.05$. The dashed curve shows the averaged mean flow $\bar{U} = \bar{u} + u_0$, i.e. the undisturbed flow plus distortion. As noted above, the flow in the experiments was far from steady, but the velocity profile measured 20 min after the forcing was introduced agrees well with figure 4 (cf. figure 10 of Delisi & Dunkerton 1989). The mean flow oscillations in the experiments suggest that the critical layer was nonlinear because the phase change across the critical layer oscillates in that case. This phenomenon is illustrated for forced Rossby waves in figures 7 and 8 of Stewartson (1981).

https://doi.org/10.1017/jfm.2013.258 Published online by Cambridge University Press

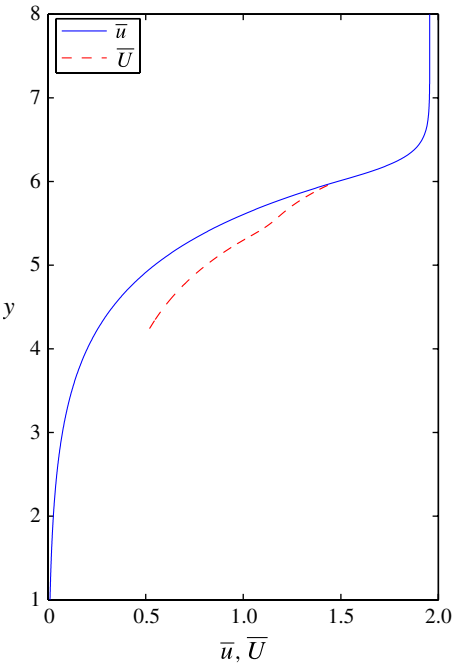


FIGURE 4. (Colour online) Mean velocity profile before and after introduction of disturbance with Richardson number $J_c = 2.52$, $Re = 3834$ and $Pr = 8$: ——, undisturbed laminar mean flow; − − −−, distorted mean flow.

4. Over-reflecting modes

The focus in this section is on modes associated with much smaller Richardson numbers than those considered in § 3. To begin, we recall that Drazin (1958) found a closed-form neutral solution for the unbounded stratified shear flow with velocity and density profiles $\bar{u} = \tanh y$ and $\bar{\rho} = \exp\{-\beta y\}$. His solution to the eigenvalue problem, (2.4), with $\bar{r} = y$ and homogeneous boundary conditions, can be written $c = 0$ and $J_c = \alpha^2(1 - \alpha^2)$. There is instability everywhere below this curve which has its maximum at $J_c = 1/4$. This was the first example of a closed-form solution for a flow with continuous velocity and density profiles and it exhibits many of the properties proved three years later by Miles (1961) to be characteristic of stratified shear flows.

The neutral and unstable eigenfunctions for the Drazin solution decay exponentially at $\pm\infty$. Some years later, the same problem was revisited by Drazin *et al.* (1979) who found additional unstable modes, which they termed unbound states. These modes have phase speeds $0 < |c_r| < 1$ and a value of α lying outside the above stability boundary, i.e. they have longer wavelengths than the neutral mode with $c = 0$ at the same value of J_0. The new modes are singular, as was the case for those with $c = 0$, but they have relatively small rates of amplification and their eigenfunctions are qualitatively different. Specifically, they owe their existence to having a region of oscillatory behaviour and the mechanism of instability is that of over-reflection, rather than the presence of an inflection point in the velocity profile.

A thorough discussion of the boundary conditions for the unbound states can be found in Drazin *et al.* (1979), but there are no details given for the specific case of the $\tanh y$ mixing layer studied as an example in their paper. We should

https://doi.org/10.1017/jfm.2013.258 Published online by Cambridge University Press

point out here then that the eigenfunction for this case is oscillatory only above the shear layer. In general, the solution above the mixing layer is of the form $v \sim R\exp(\mathrm{i}\gamma y) + \exp(-\mathrm{i}\gamma y)$, where R is the reflection coefficient. For a mode at marginal instability, the case we will look at, $R \to \infty$, so only the solution $\exp(\mathrm{i}\gamma y)$ is required. This case is termed resonant over-reflection and it has been looked at in detail in a recent paper by Benilov & Lapin (2012). With these considerations, noting that $\bar{u} \to \pm 1$ as $y \to \pm\infty$ and $\bar{r}' = 1$, the boundary conditions yielded by (2.4) are the following:

$$v \sim \exp\left[\mathrm{i}\left(\frac{J_0}{(1-c)^2} - \alpha^2\right)^{1/2} y\right] \quad \text{as } y \to \infty, \tag{4.1a}$$

$$v \sim \exp\left[\left(\alpha^2 - \frac{J_0}{(1+c)^2}\right)^{1/2} y\right] \quad \text{as } y \to -\infty. \tag{4.1b}$$

The choice of a positive sign for the exponent in the first of these conditions is consistent with the requirement that the group velocity be positive so that energy propagates outward from the mixing layer.

This has important consequences for the Reynolds stress, which must be constant for a neutral mode. It follows, however, from (4.1) that the magnitude of this constant is different above and below the mixing layer. To satisfy these conditions within the context of inviscid theory, a jump in τ is required which can occur only at the critical point. This discontinuity in τ, in reality, must be smoothed out within a diffusive critical layer and this is investigated below. To obtain the boundary conditions that we will impose on either side of the critical layer, the outer problem must first be solved by integrating the Taylor–Goldstein equation (2.4) inward from some large value of $|y|$ towards y_c. A Runge–Kutta method was used with the starting conditions provided by (4.1). For a neutral mode, α was specified and an iteration procedure employed in which c_r and J_c were varied. The solutions, after integrating inward from both boundaries, were matched at an interior point and convergence achieved when the Wronskian vanished at this interior point. Let us consider now in more detail the determination of the constants multiplying the Frobenius solutions and how they, in turn, are used to compute the rapid transition in Reynolds stress as the critical layer is crossed.

4.1. *Reynolds stress considerations near the critical layer*

Once the outer eigenvalue problem has been solved, we can obtain the information required to determine the critical layer structure from the solution for $v(y)$ above y_c. Far above the mixing layer, the initial conditions for v and v' are provided by the first of (4.1*a*) after the exponential is multiplied by C, an arbitrary complex constant. A polynomial curve fit of the solution just above y_c was then used to obtain values for the coefficients A and B of the Frobenius series (2.5); let us denote these coefficients A_+ and B_+.

The Reynolds stress can be calculated easily in the linear theory using the formula $\tau = (1/2\alpha)\,(v'v^*)_i$, where the subscript i implies the imaginary part. Because τ is a constant for a neutral mode, the following relationship, applying for $y > y_c$, can be obtained between the coefficients A_+, B_+ and C:

$$\left(\frac{J_0}{(1-c)^2} - \alpha^2\right)^{1/2} |C|^2 = \nu(A_+ B_+^*)_i. \tag{4.2}$$

https://doi.org/10.1017/jfm.2013.258 Published online by Cambridge University Press

The right-hand side of (4.2) can be obtained directly from (5.11) of Miles (1961), after noting that $X = (\mathrm{i}/\alpha)v$, where $X(y)$ describes the variation with y of the stream function. This relationship served as a useful check on the accuracy of our numerical computations.

Below the critical layer, if we use absolute values in writing the branch point terms in (2.6), the phase change of linear stability theory yields the transition relations

$$A_- = A_+ \, \mathrm{e}^{-\mathrm{i}(\pi/2)\,(1+\nu)} \quad \text{and} \quad B_- = B_+ \, \mathrm{e}^{-\mathrm{i}(\pi/2)\,(1-\nu)}. \tag{4.3}$$

(We note, in passing, that (4.3) disagrees with (25) of Eltayeb & McKenzie (1975); the results in their paper seem plausible, so hopefully this is only a typographical error.) From the behaviour of v as $y \to -\infty$, given by the second condition in (4.1*b*), it follows that $\tau = 0$ for $y < y_c$ in the case of a neutral mode. If either A or B is equal to zero, then τ will vanish everywhere; theorems VII and VIII of Miles (1961) state that this must be the case for a singular neutral mode if the velocity profile is monotonic and $\tau = 0$ at both boundaries. However, the foregoing conclusion conflicts with (4.2) above, where we have shown that in order to have a non-zero Reynolds stress on the radiating side of the shear layer, both Frobenius solutions are required. There is only one way in which all of these conditions can be accommodated and that is if

$$(A_+ B_+^* \, \mathrm{e}^{-\mathrm{i}\pi\,(1+\nu)})_i = 0. \tag{4.4}$$

This conclusion follows from Miles (1961) after setting $S(y - y_c) = 1$ in his equation (5.11), corresponding to $y < y_c$. Again, (4.4) provides a check on our computational procedure, which we found to be satisfied quite accurately even when employing a relatively large integration step size of 0.02.

4.2. *Numerical solution in the critical layer for a radiating mode*

We now present some results for the stratified mixing layer studied by Drazin *et al.* (1979). In figure 5 of their paper, results are given for an over-reflecting mode, where the curve for $c_i = 0$ was obtained by extrapolating from unstable values. Using an indented contour, we are able to compute the neutral solution directly. The upper boundary condition is given by the first of (4.1*a*), corresponding to outward radiation of energy, whereas the solution decays exponentially below the mixing layer. For a wavenumber $\alpha = 0.23$, the neutral values of phase speed and local Richardson number turn out to be $c_r = 0.04649$ and $J_c = 0.0486$, respectively.

In order to solve the system (3.3)–(3.5), the constants A and B multiplying the Frobenius solutions must be known on either side of the critical layer. To determine A_+ and B_+, we curve fit the power series (2.5) to our numerical solution of the Taylor–Goldstein equation (2.4). The jump conditions (4.3) then provide the corresponding values below the critical layer. Writing the outer expansion in inner variables, the matching conditions for $V(Y)$ can be written

$$V \sim A_+ \, Y^{(1+\nu)/2} + \hat{B}_+ \, Y^{(1-\nu)/2} \quad \text{as } Y \to \infty \tag{4.5}$$

and

$$V \sim A_- \, |Y|^{(1+\nu)/2} + \hat{B}_- \, |Y|^{(1-\nu)/2} \quad \text{as } Y \to -\infty. \tag{4.6}$$

According to the rules of asymptotic matching, only the larger of the two Frobenius solutions should be employed at lowest order. However, as discussed in § 4.1, in order to have a non-zero Reynolds stress above the critical layer both expansions must be present. To permit this formally, the constant multiplying the asymptotically smaller

https://doi.org/10.1017/jfm.2013.258 Published online by Cambridge University Press

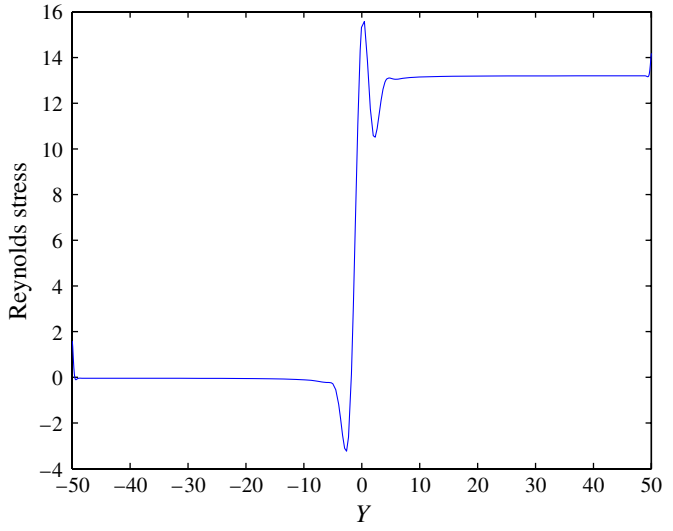


FIGURE 5. (Colour online) Variation of the Reynolds stress for a neutral mode with over-reflection in the case of a stratified mixing layer. The Richardson number $J_c = 0.0486$, the Reynolds number $Re = 1000$ and the Prandtl number $Pr = 0.72$.

solution has been rescaled by defining $\hat{B}_\pm = (\alpha\, Re)^{\nu/3} B_\pm$. The numerical solutions of the outer eigenvalue problem did, in fact, support this rescaling because the parameter ν is quite small. So, unless Re is extremely large, the assumption $(\alpha\, Re)^{\nu/3} B \sim O(A)$ is justified. (Note that the complex exponentials in (4.3) are incorporated automatically by indenting the contour of integration.)

We first show in figure 5 the Reynolds stress variation across the critical layer. As discussed above, the Reynolds stress for this case must be a non-zero constant above the critical layer, but it must decrease to zero below owing to the exponential decay of v as $y \to -\infty$. The slight overshoot on either side seems to be characteristic of τ and not due to any error, because the velocity components themselves were observed to vary smoothly and monotonically.

In figure 6, we show $|R|(Y)$ in the critical layer because, just as in the forced wave problem, the density perturbation is unbounded at the critical point unless diffusive effects are included. For the relatively small value of J_c in this case, the Frobenius solution is, in fact, more singular than it is for the forced wave problem treated in § 3. Comparing figure 6 with figure 2, there is again a peak in $|R|$ at a negative value of Y, but this time it is much closer to the centre of the critical layer. The main difference, however, is that $|R|$ is much larger above the critical layer even though the same radiation condition applies. The physics is, of course, quite different in the stability problem, where energy is radiating outward rather than being provided by a transmitted wave forced from below.

4.3. *The influence of a horizontal lower boundary*

The investigation of Drazin *et al.* (1979) was actually preceded by that of Lalas & Einaudi (1976) who considered the same flow but with a somewhat different motivation. The latter researchers cited atmospheric observations of waves much longer than what would be expected based on the results of Drazin (1958). They also pointed out that radiating modes could be a factor in the interaction of microscale dynamics with mesoscale phenomena. The presence of a lower boundary, representing

https://doi.org/10.1017/jfm.2013.258 Published online by Cambridge University Press

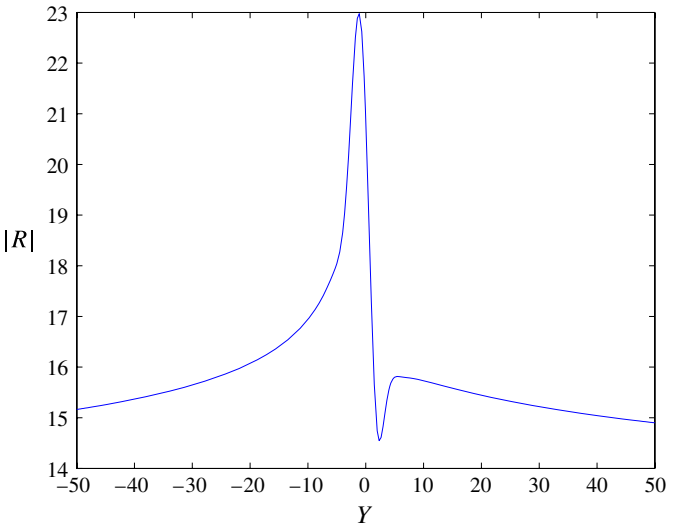


FIGURE 6. (Colour online) Variation of the modulus of the density perturbation for a neutral mode with over-reflection in the case of a stratified mixing layer. The Richardson number $J_c = 0.0486$, the Reynolds number $Re = 1000$ and the Prandtl number $Pr = 0.72$.

the Earth's surface, was shown to lead to the generation of long wave modes not present in the unbounded case. The inertial effects of density variation were also included; however, as discussed below, these are unlikely to have had a significant influence.

As in most of the paper, our interest here was initially in the role of the critical layer in over-reflection when a boundary is present and in how oscillatory modes affect the Reynolds stress distribution. Rather than determining the characteristics of many modes and dealing with a large range of parameter values, we have focused on a specific mode that seems particularly interesting. This was termed mode II in Lalas & Einaudi (1976) and it is the one closest to the stationary mode (mode I) found by Drazin (1958). Among the over-reflecting modes, this one is most pertinent to the atmosphere because instability is possible for comparatively large values of the Richardson number and the growth rates are larger than for the higher modes (termed III and IV by Lalas & Einaudi).

We have determined the stability properties for mode II using an overall Richardson number $J_0 = 0.10$ and our results agree qualitatively with those in figure 4(b) of Lalas & Einaudi (1976). Although not enough detail is given to make precise comparisons, Lalas & Einaudi do note that the eigenfunctions are oscillatory above the mixing layer for mode III, but they decay exponentially for mode II. The eigenfunctions for mode II are oscillatory between the wall and the critical point, where over-reflection occurs. Rosenthal & Lindzen (1983) have discussed the over-reflection mechanism for this configuration and derived an approximate expression relating αc_i to the reflection coefficient below the critical layer.

The mode II stability characteristics displayed in figure 7 are for three different wall locations, namely, $y_w = -10, -8$ and -6. It can be seen that the growth rates decrease and the phase speeds become more negative as the distance is reduced from the wall to the inflection point. We wished here to contrast the bounded with the unbounded case treated in § 4.2, because most of the results illustrated in Lalas & Einaudi (1976)

https://doi.org/10.1017/jfm.2013.258 Published online by Cambridge University Press

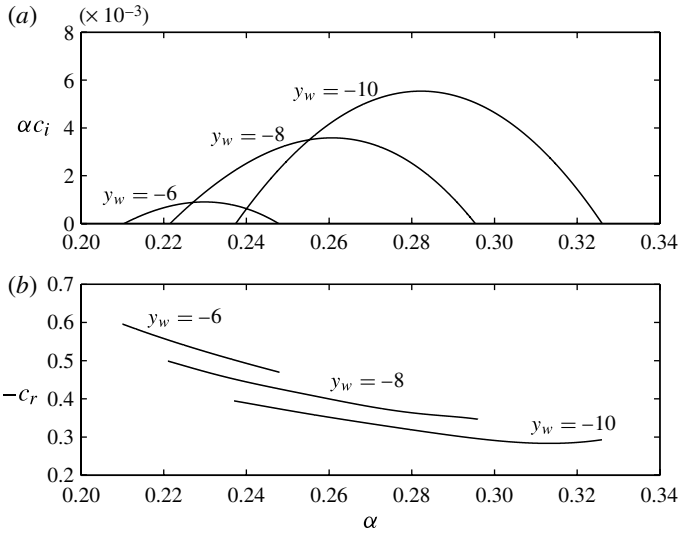


FIGURE 7. Stability characteristics for mode II of a stratified mixing layer with lower boundary y_w at the three locations indicated on the figure and unbounded above. The overall Richardson number $J_0 = 0.10$. (*a*) Amplification factor αc_i and (*b*) phase speed c_r versus wavenumber α.

were for a boundary quite far away, usually, $y_w = -10$. If the wall is too close to the shear layer, on the other hand, then mode II disappears (for $y_w < 5$).

Beginning with the growth rates in figure 7(*a*), the maximum values are comparable with those shown in figure 4(*a*) of Drazin *et al.* (1979) for $J_0/\alpha^2 = 1.5$. The difference is that the largest values of αc_i are obtained at an α more than twice as large as that of the unbounded case when the lower boundary is present. There is even more of a difference when we compare the phase speeds. First, we see in figure 7(*b*) that $|c_r|$ decreases with α which is the opposite of what happens in the unbounded case. Secondly, in the latter case, the modes are symmetric, but the effect of the lower boundary is to allow only unstable modes having negative values of c_r.

By way of quantitative comparison with Lalas & Einaudi, with $y_w = -10$ we obtain the maximum growth rate at a slightly smaller value of the wavenumber, $\alpha = 0.28$ rather than the $\alpha = 0.30$ cited in the caption of figure 9(*b*) in Lalas & Einaudi (1976). And our corresponding value of $c_i = 0.0695$ is slightly smaller than their reported $c_i = 0.07298$. One explanation that comes to mind is that Lalas & Einaudi (1976) included inertial effects, neglected in the Boussinesq approximation. However, Menkes (1959) showed that for the Drazin model the inertial terms are stabilizing. Moreover, for the values of $\beta = -\bar{\rho}'/\bar{\rho}$ utilized in the calculations of Lalas & Einaudi, the inertial terms would have little effect. In any case, what is important is that we were able to confirm the existence of the new modes reported in Lalas & Einaudi (1976), as well as their behaviour with varying α.

Returning now to the Reynolds stress distribution, as discussed in § 4.1, $\tau(y)$ can change considerably if there is a horizontal wall below the shear layer. Given that the Reynolds stress is constant for a neutral mode and that it must vanish at a boundary, it follows that $\tau = 0$ between the wall and the critical point. And, because mode II is not radiating above the shear layer, τ must then vanish above the critical layer, as well.

https://doi.org/10.1017/jfm.2013.258 Published online by Cambridge University Press

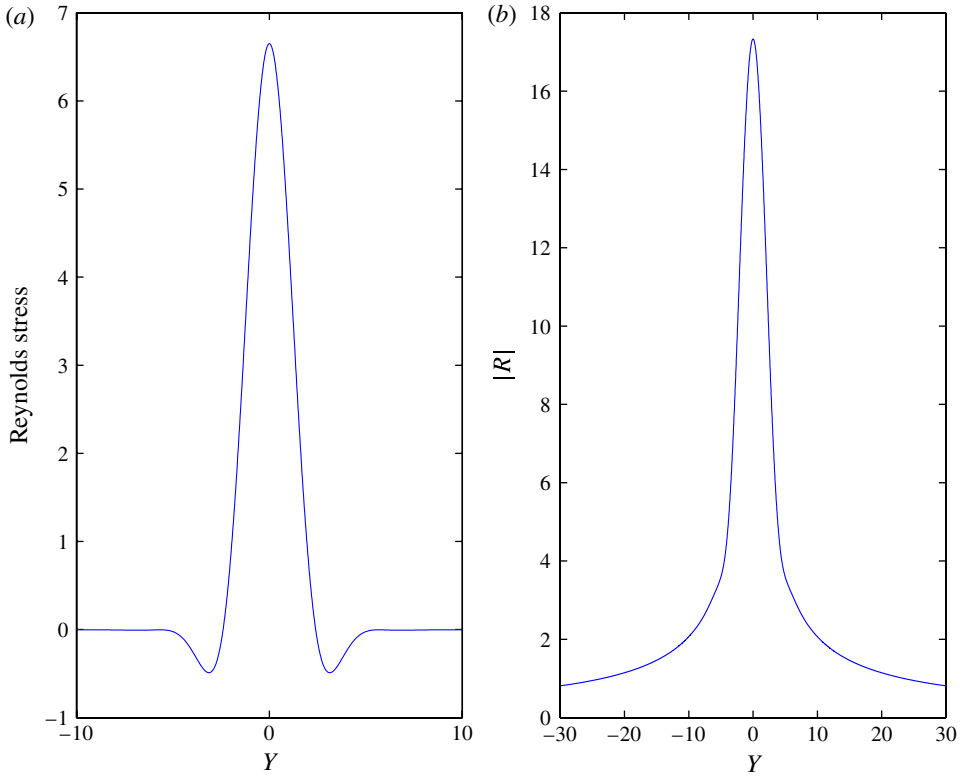


FIGURE 8. (Colour online) Variation of flow quantities across the critical layer for a neutral mode when there is a boundary below the mixing layer. The boundary is at $y_w = -8.4$ and the overall Richardson number, wavenumber and phase speed are, respectively, $J_0 = 0.10, \alpha = 0.3024$ and $c_r = -0.3329$. (*a*) Reynolds stress $\tau(Y)$ and (*b*) modulus of the density perturbation $|R|(Y)$.

Nonetheless, we will see that the Reynolds stress can be sizeable within the critical layer itself, because the horizontal perturbation velocity is singular at $y = y_c$.

We have examined both of the neutral modes for a case with $y_w = -8.4$; these occur at $\alpha = 0.225$ and $\alpha = 0.303$. Because $\tau = 0$ at both boundaries, the analysis of Miles (1961) leads to the conclusion that the eigenfunction $v(y)$ must be proportional to one or the other of the two Frobenius expansions. In this case, it turns out that $B = 0$ in (2.5) for the longer wave, whereas $A = 0$ for the shorter wave. The Reynolds stress distribution looks very similar in the two cases, so we present results in figure 8 only for the shorter wave, with $\alpha = 0.303$.

Although the computational procedure employed is essentially the same as that described in § 4.2, this case is considerably easier because there is only one Frobenius solution involved and, as a consequence, there is no dependence on the Reynolds number. From the considerations discussed above, it is not surprising that the results differ considerably from the unbounded case. Most interesting is the Reynolds stress distribution, shown in figure 8(*a*). Even though this is a neutral mode with $\tau = 0$ everywhere outside of the critical layer, we see that there is a substantial peak near its centre. The variation of the density perturbation $|R|(Y)$, shown in figure 8(*b*), also

https://doi.org/10.1017/jfm.2013.258 Published online by Cambridge University Press

differs from the unbounded case in that it is nearly symmetric about $Y = 0$. Again, this is largely because of the solution matching to only a single Frobenius expansion.

The biggest difference resulting from the presence of a lower boundary is that c_r is now always negative and its magnitude is larger than it is when the flow is unbounded. This changes a number of factors that would affect the growth rate of disturbances. Although the overall Richardson number $J_0 = 0.10$ for the case in figure 8, the local Richardson number at the critical point $J_c = 0.166$, whereas $J_0 \approx J_c$ in the unbounded case in figures 5 and 6. Despite the stabilizing effect of increasing J_c when there is a lower boundary, the amplification rates are comparable with those of the unbounded case. This is, in part, because the outward radiation of energy decreases the growth rates in the latter case.

5. The viscous critical layer for singular neutral modes on a vortex

In this section, we examine the viscous critical layer for helical modes propagating on a vortex. This is a particular case of a swirling flow, i.e. one whose velocity components in cylindrical coordinates (r, θ, z) can be written $[0, \bar{V}(r), \bar{W}(r)]$. For an incompressible flow, the governing equations are the continuity and the three momentum equations. If $(\hat{u_r}, \hat{u_\theta}, \hat{u_z}, \hat{p})$ denote the velocity and pressure perturbations, respectively, the linear normal mode theory is obtained by expressing the perturbation quantities in the form $f(r)\exp\{\mathrm{i}(kz + m\theta - \omega t)\}$. Here, k and m denote the axial and azimuthal wavenumbers and the real part of the complex quantity ω is the frequency.

The definitive paper treating the linear stability of swirling flows is by Howard & Gupta (1962). These authors were able to combine the four governing equations, after separating variables, to obtain a single ODE for $u(r)$, the r-component of the radial velocity. When $m = 0$, this second-order differential equation is the analogue of the Taylor–Goldstein equation (2.4) and a stability criterion equivalent to the Richardson number 1/4 theorem was proved by Howard & Gupta. For non-axisymmetric disturbances, however, they showed that instability is always possible for sufficiently small k/m and only a bound on the growth rate could be obtained. There are, nonetheless, mathematical similarities with the theory of stratified shear flows, even for non-axisymmetric neutral modes. Although it is no longer necessary for modes on a stability boundary to be singular, this is still usually the case. The term playing the same mathematical role as $(\bar{u} - c)$ in (2.4) was denoted γ by Howard & Gupta and its definition is the following:

$$\gamma(r) = k\,\bar{W}(r) + m\frac{\bar{V}(r)}{r} - \omega. \tag{5.1}$$

Critical point singularities can occur at any value of r where $\gamma(r) = 0$.

As in the diffusive theory of stratified shear flows, questions related to the singularity can be resolved by adding a critical layer of thickness proportional to $Re^{-1/3}$ centred on the point r_c, where γ vanishes. Only viscosity is required and the theory has been developed by Le Dizès (2004), who showed that the lowest-order pressure perturbation in the critical layer satisfies a sixth-order ODE equivalent to the one governing the vertical velocity perturbation in a stratified flow. The solution to this equation was expressed as a sum of contour integrals and their asymptotic behaviour was then used to deduce the jump conditions across the critical layer. The dependent variables in the critical layer are defined as follows:

$$U(R) = Re^{1/3}\,u(r), \quad V(R) = v(r), \quad W(R) = Re^{1/3}\,w(r) \quad \text{and} \quad P(r) = Re^{1/3}\,p(r), \tag{5.2}$$

https://doi.org/10.1017/jfm.2013.258 Published online by Cambridge University Press

where

$$R = (\gamma_c' Re)^{1/3}(r - r_c). \tag{5.3}$$

Because we wish to compute the Reynolds stress, it is more important here to solve for the radial velocity perturbation $U(R)$ than the pressure. The four critical layer equations can still be combined into a single sixth-order equation that can be written

$$\left(\frac{\mathrm{d}^3}{\mathrm{d}R^3} - \mathrm{i}R\frac{\mathrm{d}}{\mathrm{d}R} + \mathrm{i}p\right)\left(\frac{\mathrm{d}^3}{\mathrm{d}R^3} - \mathrm{i}R\frac{\mathrm{d}}{\mathrm{d}R} + \mathrm{i}(1-p)\right) U = 0, \tag{5.4}$$

where p is a Frobenius exponent for the outer problem governing $u(r)$. We will consider a specific vortex profile $\bar{V}(r)$ with no axial velocity in order to best exploit the analogy with the stratified flows investigated above. It was shown, in fact, in Caillol & Maslowe (2007) that the behaviour near the critical point r_c of $u(r)$ is exactly the same as $v(y)$ in (2.6) if we define an equivalent Richardson number by

$$J_c = \frac{2k^2 \bar{V}_c Q_c}{r_c (\gamma_c')^2}, \tag{5.5}$$

where $Q(r) = (r\bar{V})'/r$ is the vorticity of the mean flow non-dimensionalized with respect to the angular velocity at the centre of the vortex. The Frobenius exponents are then given by $p = (1 \pm \nu)/2$, where $\nu = (1 - 4J_c)^{1/2}$ for $J_c < 1/4$.

In order to compute the variation of the Reynolds stress across the critical layer, $V(R)$ must be determined in addition to $U(R)$. From the system of equations in Le Dizès (2004), a non-homogeneous ODE can be derived for $V(R)$ that can be solved once U is known, namely,

$$\frac{\mathrm{d}^3 V}{\mathrm{d}R^3} - \mathrm{i}\,R\,\frac{\mathrm{d}V}{\mathrm{d}R} - \mathrm{i}\,\frac{m\,Q_c}{r_c\,\gamma_c'}\,V = \frac{Q_c}{(\gamma_c')^{2/3}}\,\frac{\mathrm{d}U}{\mathrm{d}R}. \tag{5.6}$$

Before we can solve (5.4) and (5.6), however, the boundary conditions must be determined from the behaviour of the outer variables $u(r)$ and $v(r)$ as $r \to r_c$. To simplify our presentation of the outer problem, let us first introduce the specific case that will be analysed. This is a Lamb–Oseen vortex modified by the addition of a small term to permit the existence of singular neutral modes.

The velocity profile of the vortex that we will investigate can be written

$$\bar{V}(r) = \frac{1 - (1 - \delta r^2)\,\mathrm{e}^{-r^2}}{r}, \tag{5.7}$$

where the Lamb–Oseen vortex is recovered when $\delta = 0$. The modes of interest here were termed 'critical layer waves' by Fabre, Sipp & Jacquin (2006) in their detailed study of the Lamb–Oseen vortex. Figure 18 of their paper shows for a particular example with $m = 1$ that in one sector of the complex r-plane the solution is oscillatory on part of the real axis. We have computed the Frobenius exponent for that case and it is complex; without forcing, the perturbation is damped with $\omega = 0.1532 - 0.0221\mathrm{i}$, according to Fabre *et al.* Given that we are most interested in neutral modes on stability boundaries, we employed the profile (5.7) and found that a singular neutral mode is obtained with $\delta = 0.13$. For $\delta > 0.13$ there is instability.

In solving the Howard–Gupta equation, considerations involving the Reynolds stress were helpful and we digress briefly to note these. As in the analysis of Miles (1961) for stratified shear flows, the Reynolds stress is constant for a neutral

https://doi.org/10.1017/jfm.2013.258 Published online by Cambridge University Press

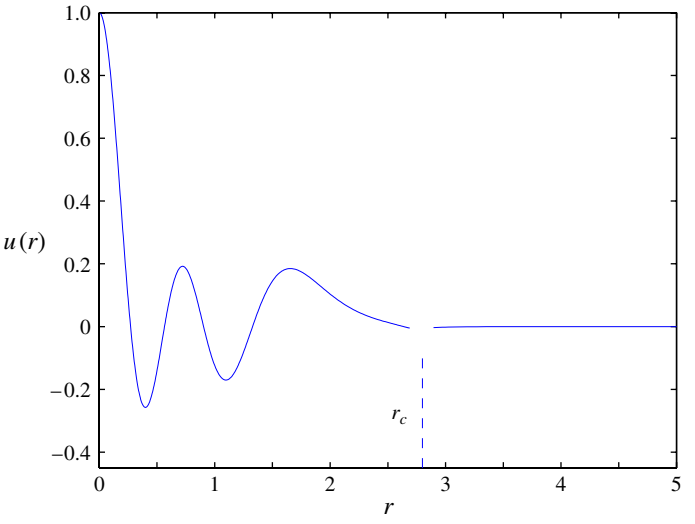


FIGURE 9. (Colour online) Radial velocity perturbation $u(r)$ for a singular neutral mode in the case of a modified Lamb–Oseen vortex, (5.7) with $\delta = 0.13$. The wavenumbers and frequency are $k = 5.0$, $m = 1$ and $\omega = 0.138$.

mode, but differences compared with the stratified case arise here owing to the cylindrical geometry. The relevant component of the Reynolds stress is now given by $\tau = -\overline{\hat{u}_r \hat{u}_\theta}$ and it was shown by Caillol & Maslowe (2007) (see their appendix A) that $\tau(r) = \tau_0/r^2$. In order for τ to be finite at $r = 0$, it is necessary that the constant $\tau_0 = 0$. In principle, τ can still be non-zero for $r > r_c$, because a discontinuity is possible at r_c. However, the Frobenius expansions, provided that p is real, rule this out and lead to the conclusion that $\tau = 0$ everywhere. It follows then that a neutral mode must be proportional to one or the other of the Frobenius series when the p_i are real.

Applying these considerations to the specific case of the profile (5.7), the neutral solution was found using a contour indented above the critical point, a consequence of γ_c' being negative for the parameter values associated with this mode. The Frobenius exponents were $p_1 = 0.227$ and $p_2 = 1 - p_1 = 0.773$ for case we chose. The numerical procedure was the same as that described in § 4 to solve the Taylor–Goldstein equation. It was found from our solution of the Howard–Gupta equation that the non-zero coefficient was the one multiplying the series beginning with $(r - r_c)^{p_2}$. If we denote the constant multiplying this series B_+, it was verified that for $r < r_c$, $B_- = \mathrm{e}^{\mathrm{i}\pi p_2} B_+$. Even though the Frobenius exponents for this case are real, it is interesting that the eigenfunction is oscillatory for $0 < r < r_c$, as shown in figure 9.

With the eigenvalue problem solved, we can now write

$$U \sim B_+ R^p \quad \text{as } R \to \infty \quad \text{and} \quad U \sim B_- |R|^p \quad \text{as } R \to -\infty, \tag{5.8}$$

where the constants $B_\pm$ can be determined from the outer solution using the procedure described at the beginning of § 4.1. Knowing the asymptotic behaviour as $R \to \pm\infty$, it is then straightforward to solve the third-order equation (5.4) with $p = p_2$ to obtain $U(R)$.

Finally, we can attack the problem of solving the non-homogeneous equation (5.6) governing the azimuthal velocity $V(R)$. The behaviour for V as $R \to \pm\infty$, according to

https://doi.org/10.1017/jfm.2013.258 Published online by Cambridge University Press

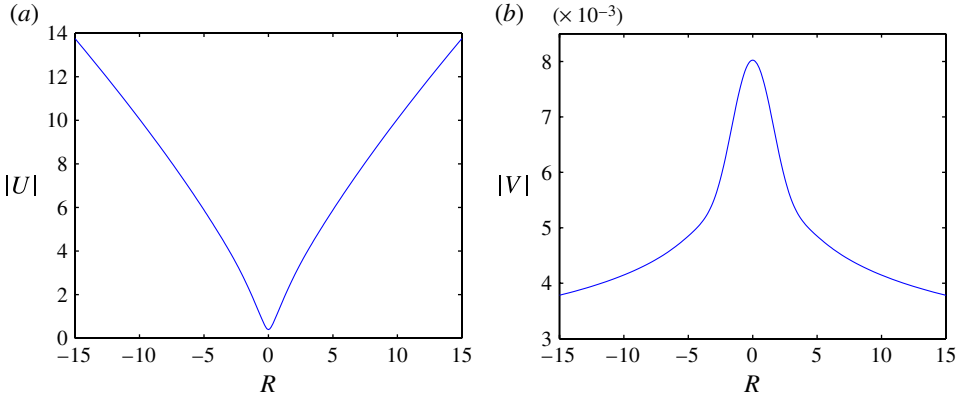


FIGURE 10. (Colour online) Critical layer variation of the radial and azimuthal velocity perturbations for a neutral mode. The basic flow is the modified Lamb–Oseen vortex (5.7) with $\delta = 0.13$. The wavenumbers and frequency are $k = 5.0, m = 1$ and $\omega = 0.138$. (*a*) Modulus of the radial velocity $|U|$; and (*b*) modulus of the azimuthal velocity $|V|$.

the outer problem, is given by $V \sim C_{\pm}|R|^{p-1}$, where

$$C_{\pm} = \pm \frac{\mathrm{i} r_c\, p\, Q_c\, (\gamma_c')^{1/3}}{m(2\,\Omega_c + p\, r_c\, \Omega_c')}\, B_{\pm}, \tag{5.9}$$

$\Omega_c = \bar{V}/r$ and B_+ is the arbitrary constant in the eigenvalue problem for $u(r)$. Imposing these conditions determines V at some initial value of $|R| \gg 1$ and we again employ a collocation method to find $V(R)$. In figure 10, the variation of the radial and azimuthal velocity perturbations $U(R)$ and $V(R)$ are shown in the critical layer. The behaviour of the outer solution suggests that $U \to 0$ near the centre of the critical layer, and figure 10(*a*) illustrates that U is indeed small, but not zero, once viscosity is taken into account.

With $U(R)$ and $V(R)$ determined, we can now compute the Reynolds stress across the critical layer. The result is illustrated in figure 11. Even though $\tau = 0$ outside the critical layer, its derivative in the r-direction is sizeable and this could produce a significant distortion of the mean velocity in the azimuthal direction. Finally, it is interesting to note the similarity with figure 8(*a*), because this variation is perhaps characteristic of problems in which the Reynolds stress vanishes outside the critical layer.

6. Concluding remarks

In the preceding three sections, we investigated the linear diffusive critical layer for a variety of flows, all of which have algebraic branch point singularities at their critical points when dissipation is ignored. Particular attention was paid to the variation of Reynolds stress because of its importance in energy exchanged between the mean flow and disturbances. The variation of quantities that become unbounded in the absence of diffusion, such as the density perturbation in a stratified flow, was also determined. We conclude now with some brief final observations about the particular cases examined.

In § 3, we re-examined the critical layer absorption associated with forced gravity waves and extended the results of Hazel (1967) to include, for example, the Prandtl number appropriate to the atmosphere. There was never any doubt about the phase

https://doi.org/10.1017/jfm.2013.258 Published online by Cambridge University Press

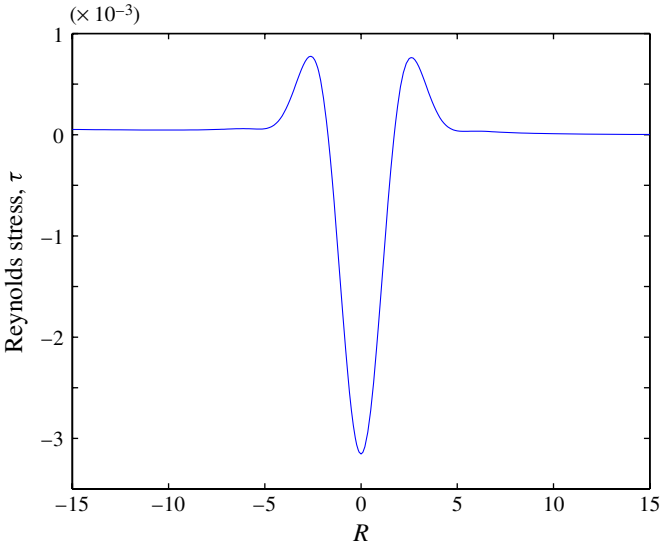


FIGURE 11. (Colour online) Distribution of the Reynolds stress across the critical layer for a vortex in the case of a modified Lamb–Oseen profile (5.7) with $\delta = 0.13$. The wavenumbers and frequency are $k = 5.0$, $m = 1$ and $\omega = 0.138$.

change across the critical layer and phenomena associated with it, so our contribution here is more on the computational side. The shooting method used in Hazel (1967) was standard at the time, but it requires six asymptotic solutions to begin the integration and to obtain these, in the words of the author, is 'straightforward, though tedious'. Because our boundary-value formulation can be used far outside the critical layer, only the behaviour of the two inviscid solutions is required. In addition, we computed the density and horizontal velocity perturbations in the critical layer. According to the outer solution, these quantities are likely to be very large in the critical layer. Finally, in § 3.2 we computed the Reynolds stress in the critical layer and the distorted velocity profile for some actual experiments with forcing at a moving boundary. It was concluded that both nonlinearity and time dependence would be required to accurately simulate the experiments. We found that the magnitude of the Reynolds stress was quite sensitive to details of the density profile.

The computations in § 4 were, perhaps, more significant because the role of the critical layer in over-reflection has been recognized for many years. Yet, the effect of diffusion on the critical layer structure and the variation of Reynolds stress have both been ignored by previous investigators. The novelty of the phenomenon and the occurrence of new modes of instability are certainly interesting mathematically. But the growth rates of over-reflecting modes are considerably smaller than the inflection point modes present at the same value of Richardson number. One reason for studying the over-reflecting modes, however, is that they can have eigenfunctions allowing radiation far outside the shear layer. A question then, deserving of further research, is to find a mechanism for their generation. Resonant interactions come to mind, because there are many new modes, especially when a lower boundary is present, as shown by Lalas & Einaudi (1976). It may even be possible to find a resonant triad, one of whose components is associated with the velocity profile, so that energy can be transferred from the faster growing inflectional mode to the radiating mode.

https://doi.org/10.1017/jfm.2013.258 Published online by Cambridge University Press

Our final example, the modified Lamb–Oseen vortex, exhibits many of the features characteristic of stratified shear flows. Critical point singularities and their effect on the variation of the Reynolds stress are significant in both cases. For the specific example we investigated in detail, the parameters were chosen so that there is a single turning point and the roots of the indicial equation are real. The properties of the eigenfunction were similar to those of one of the over-reflecting modes in a stratified mixing layer when a lower boundary is present (mode II in Lalas & Einaudi 1976). In particular, the eigenfunction was oscillatory between the critical point and the wall for the stratified flow, whereas the oscillatory region for the vortex was between the critical point and its centre. The radial variation of the Reynolds stress that we computed would modify the azimuthal velocity profile for the vortex and thereby change its stability properties. It would be interesting to see if numerical simulations of the full governing equations confirm this.

Extensions of the research on vortices could include other azimuthal velocity profiles in addition to including an axial flow. Various axial profiles should be investigated, because the axial flow $W(R)$ in the widely studied Batchelor vortex is, according to Spalart (1998), only an accurate representation of an aircraft trailing vortex far downstream.

Acknowledgements

This research was supported by the Natural Sciences and Engineering Research Council of Canada. The authors are indebted to the three referees for their careful reading of the manuscript and many suggestions for enlarging the scope of this article. Finally, we acknowledge the assistance of J. Feys in solving the outer problems for the vortex and the over-reflecting modes.

REFERENCES

BAINES, P. G. 1995 *Topographic Effects in Stratified Flows*. Cambridge University Press.

BALDWIN, P. & ROBERTS, P. H. 1970 The critical layer in stratified shear flow. *Mathematika* **17**, 513–539.

BENILOV, E. & LAPIN, V. N. 2012 On resonant over-reflection of waves by jets. *Geophys. Astrophys. Fluid Dyn.* **107**, 1–24.

BOOKER, J. R. & BRETHERTON, F. P. 1967 The critical layer for gravity waves in a shear flow. *J. Fluid Mech.* **27**, 513–539.

CAILLOL, P. & MASLOWE, S. A. 2007 The nonlinear critical layer for Kelvin modes on a vortex. *Stud. Appl. Maths* **118**, 221–254.

CAMPBELL, L. J. 2004 Wave-mean flow interactions in a forced Rossby wave packet critical layer. *Stud. Appl. Maths* **112**, 39–85.

CRAIK, A. D. D. 1985 *Wave Interactions and Fluid Flows*. Cambridge University Press.

DELISI, D. P. & DUNKERTON, T. J. 1989 Laboratory observations of gravity wave critical-layer flows. *Pure Appl. Geophys.* **130**, 445–461.

DRAZIN, P. G. 1958 The stability of a shear layer in an unbounded heterogeneous inviscid fluid. *J. Fluid Mech.* **4**, 214–224.

DRAZIN, P. G., ZATURSKA, M. B. & BANKS, W. H. H. 1979 On the normal modes of parallel flow of inviscid stratified fluid. Part 2. Unbounded flow with propagation at infinity. *J. Fluid Mech.* **95**, 681–705.

ELTAYEB, I. A. & MCKENZIE, J. F. 1975 Critical-level behaviour and wave amplification of a gravity wave incident upon a shear layer. *J. Fluid Mech.* **72**, 661–671.

FABRE, D., SIPP, D. & JACQUIN, L. 2006 Kelvin waves and the singular modes of the Lamb–Oseen vortex. *J. Fluid Mech.* **551**, 235–274.

https://doi.org/10.1017/jfm.2013.258 Published online by Cambridge University Press

GAGE, K. S. & REID, W. H. 1968 The stability of thermally stratified plane Poiseuille flow. *J. Fluid Mech.* **33**, 21–32.

GALPERIN, B., SUKORIANSKY, S. & ANDERSON, P. S. 2007 On the critical Richardson number in stably stratified turbulence. *Atmos. Sci. Lett.* **8**, 65–69.

HAZEL, P. 1967 The effect of viscosity and heat conduction on internal gravity waves at a critical level. *J. Fluid Mech.* **30**, 775–783.

HOWARD, L. N. 1961 Note on a paper of John W. Miles. *J. Fluid Mech.* **10**, 509–512.

HOWARD, L. N. & GUPTA, A. S. 1962 On the hydrodynamic and hydromagnetic stability of swirling flows. *J. Fluid Mech.* **14**, 463–476.

KIERZENKA, J. & SHAMPINE, L. F. 2008 A BVP solver that controls residual and error. *J. Numer. Anal. Ind. Appl. Maths* **3**, 27–41.

KOPPEL, D. 1964 On the stability of flow of a thermally stratified fluid under the action of gravity. *J. Math. Phys.* **5**, 963–982.

LALAS, D. P. & EINAUDI, F. 1976 On the characteristics of gravity waves generated by atmospheric shear layers. *J. Atmos. Sci.* **33**, 1248–1259.

LE DIZÈS, STÉPHANE 2004 Viscous critical-layer analysis of vortex normal modes. *Stud. Appl. Maths* **112**, 315–332.

LESSEN, M, SINGH, P. J. & PAILLET, F. 1974 The stability of a trailing line vortex. Part 1. Inviscid theory. *J. Fluid Mech.* **63**, 753–763.

LINDZEN, R. S. & BARKER, J. W. 1985 Instability and wave over-reflection in stably stratified shear flow. *J. Fluid Mech.* **151**, 189–217.

MASLOWE, S. A. 1986 Critical layers in shear flows. *Annu. Rev. Fluid Mech.* **18**, 405–432.

MENKES, J. 1959 On the stability of a shear layer. *J. Fluid Mech.* **6**, 518–522.

MILES, J. W. 1961 On the stability of heterogeneous shear flows. *J. Fluid Mech.* **10**, 496–508.

ROSENTHAL, A. J. & LINDZEN, R. S. 1983 Instabilities in a stratified fluid having one critical level. Part II. Explanation of gravity wave instabilities using the concept of overreflection. *J. Atmos. Sci.* **40**, 521–529.

SPALART, PHILIPPE. R. 1998 Airplane trailing vortices. *Annu. Rev. Fluid Mech.* **30**, 107–138.

STEWARTSON, K. 1981 Marginally stable inviscid flows with critical layers. *IMA J. Appl. Maths* **27**, 133–175.

STUART, J. T. 1963 Hydrodynamic stability. In *Laminar Boundary Layers* (ed. L. Rosenhead), chap. 9. Oxford University Press.

https://doi.org/10.1017/jfm.2013.258 Published online by Cambridge University Press